LBL-32590
UC-401
Preprint

Lawrence Berkeley Laboratory
UNIVERSITY OF CALIFORNIA

CHEMICAL SCIENCES DIVISION

Submitted to Journal of Chemical Physics

Resonance-Enhanced One- and Two-Photon Ionization of Water Molecule: Preliminary Analysis by Multichannel Quantum Defect Theory

M.J.J. Vrakking, Y.T. Lee, R.D. Gilbert, and M.S. Child

July 1992

LBL-32590
Copy 1
REFERENCE COPY
Does Not
Circulate
Bldg. 50 Library.

Prepared for the U.S. Department of Energy under Contract Number DE-AC03-76SF00098

DISCLAIMER

This document was prepared as an account of work sponsored by the United States Government. While this document is believed to contain correct information, neither the United States Government nor any agency thereof, nor the Regents of the University of California, nor any of their employees, makes any warranty, express or implied, or assumes any legal responsibility for the accuracy, completeness, or usefulness of any information, apparatus, product, or process disclosed, or represents that its use would not infringe privately owned rights. Reference herein to any specific commercial product, process, or service by its trade name, trademark, manufacturer, or otherwise, does not necessarily constitute or imply its endorsement, recommendation, or favoring by the United States Government or any agency thereof, or the Regents of the University of California. The views and opinions of authors expressed herein do not necessarily state or reflect those of the United States Government or any agency thereof or the Regents of the University of California.

LBL-32590
UC-401

RESONANCE-ENHANCED ONE- AND TWO-PHOTON IONIZATION OF WATER MOLECULE: PRELIMINARY ANALYSIS BY MULTICHANNEL QUANTUM DEFECT THEORY

Marcus J.J. Vrakking and Y. T. Lee

Department of Chemistry
University of California
and
Chemical Sciences Division
Lawrence Berkeley Laboratory
Berkeley, CA 94720 USA

and

Richard D. Gilbert and Mark S. Child

Department of Theoretical Chemistry, University of Oxford,
5 South Parks Road, Oxford OX1 3UB, United Kingdom

July 1992

This work was supported by the Director, Office of Energy Research, Office of Basic Energy Sciences, Chemical Sciences Division, of the U.S. Department of Energy under Contract No. DE-AC03-76SF00098.

ABSTRACT

Experimental results are presented for one- and two-photon ionization of the water molecule, obtained using a near transform-limited xuv laser. The single-photon ionization results show rotationally resolved auto-ionizing resonances corresponding to members of Rydberg series (nd <-- $1b_1$; n = 6-11) converging on the $H_2O^+(100)$ vibrational state. The (1+1) multi-photon ionization results show rotationally resolved structure corresponding to Rydberg series (nd <-- $1b_1$; $n \geq 6$) converging on the $H_2O^+(000)$ vibrational state. Typical linewidths below and above the $H_2O^+(000)$ ionization threshold are 1 cm^{-1} and 2 cm^{-1}, respectively.

The experimental results are simulated by multichannel quantum defect theory (MQDT). The main features in the spectrum are reproduced in a treatment of the rotational channel interactions with partial *l* mixing. It is argued that remaining discrepancies between experiment and theory arise from perturbative interactions between the (nd <-- $1b_1$) levels and members of the (nd <-- $3a_1$) Rydberg series. Also, it is argued that in the (1+1) multi-photon ionization spectra lines may be missing due to selective predissociation.

1. Introduction

In recent years, the photoionization spectrum of the water molecule has become the model system of choice for the treatment of the Rydberg spectra of a polyatomic molecule by multichannel quantum defect theory (MQDT). Photoionization spectra obtained by Page et. al.[1] first showed a number of auto-ionizing Rydberg series converging on the (100) vibrational state of the H_2O^+ ion in its ground electronic state, and this provided the impetus for Child and Jungen to carry out the first MQDT calculation for an asymmetric top molecule[2].

The results of Page et. al. showed resolved rotational structure for principal quantum number n = 6, which is the lowest member of these Rydberg series above the (000) ionization threshold, but for higher members of the Rydberg series only the very strongest rotational features could be observed. Recent improvements in the generation of extreme ultra-violet radiation (xuv) have enabled an experiment where the rotational structure of the H_2O Rydberg series can be followed to higher principal quantum number, with the additional advantage of improved resolution. These new spectra are presented in this paper.

In addition, results are presented for an experiment where H_2O Rydberg series converging on the (000) vibrational state of the H_2O^+ ion were studied by employing a (1 + 1) multi-photon ionization (MPI) technique. These Rydberg series are expected to have quantum defects very similar to the series observed in the direct photoionization experiment, and thus their observation aids in the assignments of the photoionization spectra. Furthermore, differences between these MPI spectra and the photoionization results give information about the decay mechanisms of the Rydberg states and the extent to which these states are perturbed by neighbouring states.

Efforts were made to simulate the spectra using multichannel quantum defect theory[3-5], with a description in terms of rotational channel interactions with partial l mixing. Although the simulations were able to reproduce some of the main features of the spectra, some serious discrepancies remain. It is believed that these discrepancies are due to perturbations by overlapping excitations to linear ionic states.

H_2O Rydberg Spectroscopy

The molecular orbital structure of the H_2O molecule in its ground state is given by $X^1A_1\{(1a_1)^2\ (2a_1)^2\ (1b_2)^2\ (3a_1)^2\ (1b_1)^2\}$. In the spectral range of interest in this paper absorption features are observed corresponding to excitation of electrons in the $3a_1$ and the $1b_1$ orbitals, which are a bonding orbital in the molecular plane and a nonbonding oxygen p-orbital pointing out of the molecular plane, respectively. Removal of an electron in the $1b_1$ orbital forms the H_2O^+ ion in the X^2B_1 ground state, which has a bent geometry close to the initial H_2O geometry. Removal of an electron from the $3a_1$ orbital forms the H_2O^+ ion in the A^2A_1 state, which is linear, and the large geometry change induces long progressions in the bending vibration. In the current paper we will mainly be concerned with excitations of the $1b_1$ orbital.

The first observation of members of the $(1b_1)^{-1}$ Rydberg series discussed in this paper was done by Price[6], who measured members of four different Rydberg series labelled A, B, C and D, which were later interpreted as excitation from the non-bonding $1b_1$ orbital to orbitals with symmetry npa_1 (A), npb_1 (B), nda_1 and nda_2 (C), and ndb_1 and nda_1' (D) [7]. The quantum defects of these states are close to the quantum defects of a single oxygen atom, namely $\mu \approx 1.4$ for the ns series, $\mu \approx 0.7$ for the np series and $\mu \approx 0$ for the nd series, which matches reasonably well the oxygen atom quantum defects of 1.20, 0.76 and 0.03 respectively[8]. In subsequent experiments the absorption and photoionization spectrum have been determined with increasing precision. In what follows, we will focus primarily on the observation of members of Rydberg series with principal quantum number $n \geq 6$.

Using a helium continuum source, Katayama et.al.[9] measured the total absorption and photoionization cross section in the wavelength range from 580 to 1050 Å with a resolution of 0.5 Å, and were able to observe Rydberg series up to principal quantum number $n=8$. For these higher principal quantum numbers the spectrum is dominated by excitation to nd orbitals. Since the $1b_1$ orbital is essentially an atomic p-orbital, the $\Delta l = \pm 1$ selection rules forbids excitation to p-orbitals unless the np Rydberg orbital is perturbed by the molecular core, as is the case for low principal quantum numbers. For higher principal quantum numbers the np <-- $1b_1$ transition becomes nearly forbidden. Ab-initio

calculations by Diercksen et.al.[10] show that the oscillator strength for excitation to nd levels is significantly larger than for excitation to ns levels, so to a good approximation the Rydberg series observed in the current experiments can be described as being due exclusively to nd <-- $1b_1$ excitations. Using synchrotron radiation Ishiguro et.al.[11] and Gürtler et.al.[12] measured the absorption spectrum between 600 Å and 1250 Å, with a resolution of 0.03 Å in the latter experiment, and were able to determine the positions of the nd series out to principal quantum number n=13.

There are five different nd orbitals for each principal quantum number, namely nda_1 (σ^+), ndb_2 (π^+), nda_2 (π^-), nda_1' (δ^+) and ndb_1 (δ^-). Following the standard approach to evaluate the non-zero transition matrix elements for a dipole-allowed transition[13], a transition moment along the x-axis (c-axis) transforms as b_1 and therefore c-type transitions (ΔK_a = odd, ΔK_c = even) are allowed to nda_1 orbitals. A transition moment along the y-axis (a-axis) transforms as b_2 and therefore a-type transitions (ΔK_a = even, ΔK_c = odd) are allowed to a_2 orbitals. And finally, a transition moment along the z-axis (b-axis) transforms as a_1 and therefore b-type transitions (ΔK_a = odd, ΔK_c = odd) are allowed to b_1 orbitals. There are no dipole-allowed transtions to orbitals of b_2 symmetry.

The quantum defect treatment of Child and Jungen showed that for high principal quantum numbers, in the limit of *l*-uncoupling, when the Rydberg electron is more appropriately described in a space-fixed coordinate system (Hund's case (d)) than in a molecule-fixed coordinate system (Hund's case (b)), the frame transformation from case (b) to case (d) results in an alternative set of propensity rules[2]:

$$\begin{aligned} \lambda'' \ even/odd &\leftrightarrow K_a^+ - K_a'' \ even/odd \\ p_e'' + \lambda'' + 1 \ even/odd &\leftrightarrow K_c^+ - K_c'' \ even/odd \end{aligned} \qquad (1)$$

where λ'' is the projection of the orbital angular momentum *l* in the molecular frame in the ground electronic state and p_e'' is the parity of the electronic wavefunction in the ground electronic state . For the $1b_1$ lone pair orbital of the H_2O molecule, one has $\lambda'' = l'' = 1$ and

$p_c'' = 0$, leading to ΔK_a = odd and ΔK_c = even, which corresponds to c-type transitions. In the Rydberg spectra of the H_2O molecule a change in appearance is therefore anticipated between transitions to Rydberg levels with low principal quantum numbers, where a-type, b-type and c-type transitions are observed, and to Rydberg levels with high principal quantum numbers, where only the c-type transitions are expected to occur, and where consequently the number of observed rotational transitions will be reduced, in apparent agreement with the results of Page et. al.[1].

Measurements of H_2O Rydberg spectra with rotational resolution have been limited sofar. Fairly extensive data is available for the 3d complex[14, 15, 16, 17], and in fact a theoretical analysis for this portion of the spectrum was recently published[18]. For Rydberg excitations with higher principal quantum numbers to date the only published spectra with rotational resolution remain the photoionization results of Page et.al.[1], which, using an extreme ultra-violet (xuv) laser with a 1.5 cm^{-1} bandwidth, show peaks corresponding to auto-ionization of individual rotational features of several Rydberg series converging on the (100) vibrational state of H_2O^+. The spectra published by Page et.al. show a fair amount of rotational structure for principal quantum number n=6, whereas for higher principal quantum numbers a significant amount of the rotational structure is lost in the continuum background.

Tonkyn et.al.[19] have recently published the rotationally resolved threshold photoionization spectrum of the H_2O molecule by using pulsed-field ionization of extremely high-n Rydberg states ($n \geq 150$). This spectrum shows the convergence limits for individual rotational transitions. A simulation of the intensities observed for different final rotational states of the H_2O^+ ion revealed that the Rydberg excitation is described by a combination of a-type and c-type transitions. Possible explanations for the occurrence of a-type transitions, which contradict the above propensity rule, include *l*-mixing in the initial $1b_1$ orbital or in the nominal nd orbital. Tonkyn et.al.[19] favoured the former, but this is ruled out by Gilbert and Child[20] on grounds that the np<--$1b_1$ ZEKE spectrum arising from a d component in the initial orbital occurs at a higher frequency than the observed nd<--$1b_1$ spectrum. Ab initio based studies by Lee et.al.[21] show conclusively that the main source of a-type intensity is *l*-mixing in the excited photoorbital. The dipole perturbation model

offered by Gilbert and Child[20], which reaches the same conclusion by a different route, attributes the high intensity of the a-type ZEKE lines to intensity borrowing from moderate n=50 members of the allowed nd<--$1b_1$ series which are imbedded in the dense near continuum of an np series terminating on a lower rotational level of the positive ion. Resonant mixing of this type is unlikely to affect the present low n=10 region of the spectrum, but persistent weak *l*-mixing can have a more subtle effect by altering the orbital composition of the excited state and hence breaking the propensity rule in Equation (1).

Wang et.al.[22] have observed how in portions of the spectrum intensity is missing for excitation from the $1b_1$ orbital to ns, np and nd orbitals of a_1 symmetry. They speculated that this is due to dynamic Renner-Teller interactions between bent and linear states with different values of the principal quantum number but similar energies. A recent paper by Hirst and Child[23] supports this idea. Hirst and Child calculated ab-initio bending potential curves for Rydberg states of H_2O up to energies of about 12 eV. Their results indicate that the bending potentials contain a large number of avoided crossings between diabatic curves corresponding to bent states, describing excitation of the $1b_1$ non-bonding orbital and diabatic curves corresponding to linear states, related to excitation of the $3a_1$ bonding orbital. Interactions with the $3pb_2$<--$3a_1$ ($^1B_2$) linear state, for which seveal low-lying bending levels have been reported[24], are predicted to be particularly important, because the avoided crossing are predicted to lie close to all nda_2<--$1b_1$ ($^1B_2$) potential minima and a strong perturbation of this type has already been observed in the E' band of the 3d<--$1b_1$ cluster[18].

Once formed, the fate of the Rydberg molecule depends strongly on whether its total energy does or does not exceed the ionization threshold. Levels below the ionization threshold are predissociated by the B^1B_1 state and the asymptotic channels which are energetically accessible are[25] $OH(X^2\Pi)$ + H(n=1), $OH(A^2\Sigma^+)$ + H(n=1), $H_2(^1\Sigma_g^+)$ + $O(^3P)$, $H_2(^1\Sigma_g^+)$ + $O(^1D)$ and $O(^3P)$ + 2 H(n=1). For example, at an excitation energy of 10.2 eV 78 % of the Rydberg molecules decay into H + OH, 12 % into H + H + O and 10 % into H_2 + O [26]. Above the ionization threshold auto-ionization becomes a major decay channel and Dutuit et. al.[25] observed an approximately 50 % drop in the fluorescence of the $OH(A^2\Sigma^+)$ state around the ionization threshold.

Multichannel Quantum Defect Theory

The conventional Born-Oppenheimer approach to molecular spectroscopy is no longer applicable in the Rydberg region, because the electronic energy separations eventually become small compared with vibrational and even rotational level separations. Instead the method of choice is multichannel quantum defect theory[3-5], which treats the short range interactions in terms of scattering of the Rydberg electron from the positive ion core and then imposes different boundary conditions according to whether the relevant channels are open or closed at the energy of interest. The high electron kinetic energy in the core region allows considerable simplification first because the high local electron velocity is consistent with a Born-Oppenheimer picture in which the short-range scattering phase shifts, which are expressed in terms of quantum defects, may be taken to be diagonal with respect to body fixed components of the wavefunction. In other words Hund's case (b) angular momentum coupling is taken to apply at short range. A second simplification, due to the fact that the kinetic energy close to the core vastly exceeds the energy range of typical interest, is that the quantum defects may be taken, as a first approximation, to be independent of energy. Finally the high short range electron velocity is taken to justify a sudden recoupling of the angular momentum to space fixed axes as the electron recedes to long range, where Hund's case (d) applies. The upshot is that the short-range scattering matrix is expressed in the energy independent form

$$S_{ii'} = \sum_{\alpha} \langle i \mid \alpha \rangle e^{2i\pi\mu_\alpha} \langle \alpha \mid i' \rangle \qquad (2)$$

where $|i\rangle$ and $|i'\rangle$ are Hund's case (d) states, the $|\alpha\rangle$ are case (b) states and μ_α are the quantum defects.

Child and Jungen[2)] have given a detailed exposition of the theory of rotational channel interactions (i.e. excluding vibrationally inelastic short range scattering) within the approximation of pure precession, which implies a transition from a Hund's case (b)

spectrum at low principal quantum numbers where the electronic energy separation normally exceeds the rotational constants, to a Hund's case (d) spectrum at high n values such that the energy separations within a given l manifold become negligible compared with the rotational constants. This is however an oversimplification because the effects of l-mixing can seldom be ignored. One consequence is to break the pure precession propensity rules in the case (d) limit as seen for example by the influence of d/p mixing in allowing[20,21] the appearance of type a lines in the afore-mentioned pulsed-field ionization spectrum of H_2O [19]. Secondly, l mixing can significantly alter Coriolis coupling strengths and hence delay the complete transition to case (d) frequency separations until the case (b) electronic origins for all l waves at given n are effectively degenerate on the scale of the rotational constants.

Further complications which remain to be incorporated within MQDT for polyatomic molecules include vibrational and electronic channel coupling. The former clearly drives the autoionization process responsible for detection of the nd(100) <-- $1b_1$ series in H_2O first observed by Page et. al.[1] and now reported in higher resolution below. The presence of vibronic coupling in the H_2O^+ positive ion[27] may also be expected to give rise to perturbations between the nd <-- $1b_1$ series and bending levels of the various $3l$ <-- $3a_1$ linear states. One such perturbation was identified by analysis of the 3d cluster[18] and others are predicted in a recent ab initio study[23].

The current neglect of these complications makes it impossible to give a complete account of the observed spectra, but some pointers towards the interactions at play are given.

2. Experimental Approach

The experimental apparatus used in this experiment consisted of a near-perpendicular crossed beam arrangement of an extreme ultra-violet (xuv) laser and a pulsed molecular beam, which will now be described in turn.

Pulsed xuv radiation was generated by frequency-upconversion of the output of a near transform-limited visible dye laser system, which is based on pulse-amplification of the continuous output of a Coherent 699-29 Autoscan ringlaser in four stages, using three prism dye amplifiers, where the second dye amplifier is double-passed[28]. The dye-amplifiers are pumped by the second harmonic of a Quantel Nd:YAG laser model 581C. At a 600 nm wavelength this laser system is capable of generating up to 120 mJ in a 7 nsec FWHM pulse with a near transform-limited bandwidth of 91 MHz. The laser operates at a 10 Hz repetition rate.

The dye laser output was frequency-doubled using KDP crystals, generating in excess of 30 mJ/pulse of ultra-violet radiation. This ultra-violet radiation was focussed onto a pulsed Ar jet using a 25 cm focal length fused silica lens and xuv radiation was obtained by frequency tripling[29]. A home-built pulsed valve according to the design of Proch and Trickl[30] was used to generate the pulsed Ar jet, and was operated with a 50 psig Ar backing pressure behind a 1 mm nozzle. The tripling chamber was differentially pumped by a 6" Varian cryopump. The xuv output of the entire laser system was calibrated by Cromwell et.al. at 98 nm, where it was reported to exceed 10^{11} xuv photons/pulse[28]. The bandwidth of the xuv laser was experimentally determined to be 210 MHz by studying (1+1) photoionization of Kr atoms[31].

The xuv radiation passed through a 1 meter McPherson Model 225 vuv monochromator, which served two purposes. First of all, by operating the grating in first order, the monochromator allowed separation of the xuv and the co-propagating ultra-violet radiation, so the direct photoionization experiments could be carried out without the possibility of multi-photon interferences from the ultra-violet, which is about five orders of magnitude more intense than the xuv light. And secondly, the grating serves to refocus the xuv radiation, which is strongly divergent as it exits the tripling region. Since the tripling jet

is located outside the monochromator, the xuv radiation is refocussed inside the monochromator when a standard grating for this monochromator is used, and at the crossing point with the molecular beam in the main chamber the xuv beam size is about 3 mm, which approximately matches the size of the molecular beam. This is the condition under which the direct photoionization measurements were performed.

In the (1+1) multi-photon ionization (MPI) experiments the grating was operated in zeroth order, where the ultra-violet light which had been used to generate the xuv radiation served to ionize the Rydberg molecule. In order to achieve this it was necessary however to change the experimental arrangement a little. The H_2O Rydberg states studied in this experiment are rapidly predissociated, with lifetimes of about 10 picoseconds. If the ultra-violet light is refocussed into a 3 mm spot the ionization rate of the Rydberg molecules is too low to give a detectable signal, and therefore the 1 meter focal length grating was replaced by a 1.188 meter focal length grating which was mounted off the backflange of the vuv monochromator and manipulated in such a way that the xuv and ultra-violet were refocussed at the molecular beam. The MPI signals that were obtained in this fashion were up to ten percent of the signals in the direct photoionization experiment.

The pulsed H_2O molecular beam was generated by using a second pulsed valve according to the design of Proch and Trickl[30]. The H_2O sample was held at O °C, and expanded through a 1 mm nozzle in 150 Torr of Ne carrier gas. The pulsed valve was located inside a separate source chamber, and the pulsed molecular beam was formed by skimming the pulsed H_2O jet 4 cm from the nozzle with a 2 mm ID skimmer. The distance from the nozzle to the laser axis was about 8 cm. The rotational temperature of the H_2O beam is not accurately known, but is probably not too different from the 30 K temperature quoted in the experiment of Page et. al.[1] In the simulations to be discussed in the next section a 25 K beam temperature was assumed. Ions formed at the crossing point of the laser and the molecular beam were mass selected by time-of-flight and detected by using a Daly-type detector. The signal from the detector was fed into a boxcar averager and stored on the Autoscan computer.

Shot-to-shot fluctuations in the xuv laser power can easily be as much as 50 %, and therefore, in order to obtain a good signal-to-noise ratio in the direct photoionization

experiment, a normalization procedure for the xuv laser power was required. Similar to Page et. al.[1] C_2H_2 was mixed in with the Ne carrier gas to provide a nearly wavelength independent ionization signal with the same laser power dependence as the H_2O photoionization signal. The H_2O^+ and $C_2H_2^+$ signals were averaged separately on two boxcar averagers and the ratio, determined by an analog processor, was used as a true measure of the H_2O photoionization efficiency. In order to achieve the optimum linearity for the normalization procedure, the Ne/C_2H_2 mixture was prepared with a Ne : C_2H_2 partial pressure ratio of about 100 : 1, which resulted in similar signal levels at the H_2O^+ and $C_2H_2^+$ peaks. The single shot variations in the normalized signal were about 20 %, with no residual correlation to the xuv laser power. Spectra were recorded by scanning the Autoscan ringlaser and averaging the signal obtained from 30 lasershots. All scans were repeated 3-5 times, and thus the photoionization spectrum was obtained with a signal-to-noise ratio of about 50:1, allowing many weak rotational features, which could not be observed before in the experiment of Page et. al.[1], to be resolved. It should be mentioned that the normalization with C_2H_2 also takes care of the wavelength dependence of the laser power and the Ar tripling efficiency.

In the MPI experiment, the C_2H_2 can be ionized either by absorption of a single xuv photon or by absorption of three or more photons from the ultra-violet laser which co-propagates with the xuv laser. When the efficiency of the xuv generation was optimized, it was found that the signal for the direct photoionization by one xuv photon was about 15 times stronger than the latter MPI process, and therefore the MPI spectra were recorded applying the normalization as well. Once an H_2O^+ signal was found in the MPI experiment, the location of focus of the xuv laser was fine-adjusted by simultaneously moving the nozzle of the Ar jet and the 25 cm lens which focusses the ultra-violet light onto the jet along the laser propagation axis.

3. Results and Analysis

(1+1) Multi-photon ionization (MPI) spectra were recorded from 98550 cm^{-1} up to the ionization threshold at 101766 cm^{-1} [19], corresponding to the frequency range of the Rydberg series (nd <-- $1b_1$; $n \geq 6$), converging on the (000) vibrational state of H_2O^+. A typical portion of the spectrum, showing absorption features in the spectral region of the nd <-- $1b_1$ transitions, is reproduced in the upper panel of Figure 1a. Single-photon ionization spectra were recorded from 101610 cm^{-1} to 104120 cm^{-1}, corresponding to the frequency range of the autoionizing Rydberg series (nd <-- $1b_1$; n = 6-11), converging on the (100) vibrational state of H_2O^+ at 104979 cm^{-1}. A typical section of the spectrum, showing the photoionization efficiency in the vicinity of the nd <-- $1b_1$ transitions, is shown in the upper panel of Figure 2a. Positions and intensities for the dominant observed transitions are summarized in Tables 1 and 2, along with results of the quantum defect calculations to be described below.

In relation to Figures 1a and 2a, a few introductory remarks can be made. First of all the direct photoionization and the MPI spectrum have a significant number of lines in common, illustrating the fact that (i) the quantum defects for the direct photoionization and the MPI experiment should be quite similar, and (ii) the rotational structure for $H_2O^+(000)$ and $H_2O^+(100)$ is almost identical. The differences between Figures 1a and 1b point towards perturbations affecting the 6d levels in one or both of the Rydberg series and towards differences in the decay mechanisms for the 6d members of both series.

In the MPI results in Figure 1a the linewidths are typically O(1 cm^{-1}), whereas in the photoionization results the linewidths are typically O(2-3 cm^{-1}). This is consistent with the fact that below the ionization threshold the linewidth is determined predominantly by the lifetime towards predissociation, whereas above the ionization threshold the linewidth is determined by the competing processes of auto-ionization and predissociation. This result is consistent with the experiments of Dutuit et. al.[25] which were mentioned in the introduction.

As noted by Page et.al.[1], for each principal quantum number value, the spectra tend to be dominated by two peaks, which Page et. al. labelled 'a' and 'b' in their photoionization

spectra. From their MQDT calculation[2)] Child and Jungen concluded that the a-series corresponded to excitation from the 1_{01} ground rotational state to a Rydberg level corresponding predominantly to a 1_{11} ionic rotational state, whereas the b-series corresponded to excitation from the 1_{01} ground rotational state to a Rydberg level corresponding predominantly to a 2_{11} ionic rotational state. In the current experiment the na-nb series can be followed to n=13 in the MPI results and to n=11 for the direct photoionization results.

It is interesting to look at the linewidths of the peaks of the na/nb series. In the current experiments the laser bandwidth is negligible compared to any of the observed linewidths and therefore these linewidths give a direct determination of the lifetime of the Rydberg level which is excited. This statement is also valid for the MPI experiment where an estimated 95% of the excited molecules decayed via predissociation. The observed linewidths are collected in Table 3. As expected, the linewidths for the Rydberg series converging on the $H_2O^+(000)$ vibrational state are lower than those for the Rydberg series converging on the $H_2O^+(100)$ vibrational state. Also, it is observed that the lines generally become narrower with increasing principal quantum number, reflecting the reduced core-penetration of the Rydberg orbital for highly excited Rydberg orbitals. Table 3 shows enhanced linewidths for some selected lines. These enhanced linewidths could in principle provide valuable information about interactions perturbing the Rydberg levels, such as interactions with linear states involving excitations of the $3a_1$ orbital.

Quantum Defect Analysis

The observed MPI and photoionization spectra, together with a tentative multichannel quantum defect simulation[2)], based on assignment to the nd(000) <-- $1b_1$ and nd(100) -- $1b_1$ series respectively, are shown in Figures 1 and 2. Minor differences between the two series are to be expected from differences in the quantum defects, since in the two series the electron-core collisions sample a slightly different range of ion-core geometries. The observed discrepancies are however too numerous and too unsystematic to be accounted for in this way, because in any case the simulated spectra for $n \geq 9$ are found to depend only

on the composition of the channel wavefunctions (see below) and the H_2O^+ rotational constants, and hardly at all on any reasonable choice of the quantum defects.

One obvious feature is that the n=7 and n=8 photoionization bands are heavily overlapped by other band systems, which might include bending levels of one or more of the 3d <-- $3a_1$ linear states as suggested by Page et.al.[1] or of the 3p <-- $3a_1$ linear states. In particular it should be noted that lower bending levels of the $3pb_2$ <-- $3a_1(^1B_2)$ linear state have already been reported[24], that one of them not only overlaps but also perturbs the 3d cluster[20] and that other possible interactions between the $3pa_1$ <-- $3a_1(^1A_1)$ and $3pb_1$ <-- $3a_1(^1B_1)$ linear states and higher members of the nd <-- $1b_1$ series are suggested by a recent ab initio study[23].

A second possible explanation for the observed differences between Figures 1 and 2 lies in the method of detection, because lines may be lost from the MPI spectrum by rotationally selective predissociation, which is well attested elsewhere in the spectrum[20,24]. Similar loss is however less likely from the photoionization series because the autoionization quantum yield is known to exceed that for predissociation[25]. Such selective predissociation could for example account for the intensity difference between the strong feature in the n=6 photoionization spectrum (labelled b in Figure 2(a) after Page et.al.[1]) and the much weaker 'b' feature in the n=6 MPI band. It is also difficult to account for the absence of strong 'a' feature lines in the MPI series for n = 10-12 except by the opening up of a predissociation channel.

Turning to the details of the simulation, there is evidence for significant l mixing in the fact that the spacings of the 'a' and 'b' peaks in the n = 9-11 members of the photoionization series are markedly less than the 2_{11} <-- 1_{11} level separations in the simulated nd <-- lb_1 case (d) spectrum in Figure 2(g). This can be understood in the following way. In the Watson Hamiltonian[32] the case (b) terms $|JlK\lambda>$[18] are Coriolis coupled by the terms $J_a l_a$, $J_b l_b$ and $J_c l_c$. However, if what is nominally a $|d\sigma>$ orbital is actually an s/d admixture

$$|d\sigma\rangle = \cos\theta\ |20\rangle + \sin\theta\ |00\rangle \qquad (3)$$

then any Coriolis coupling within the d manifold is diminished by a factor $\cos\theta$. In the present case, the necessary reduction in Coriolis coupling to account for this diminished strong peak separation was most simply accommodated by allowing an admixture of s character into the $d\sigma$ orbital, with a mixing angle of 0.1π. Supporting evidence comes from the fact that such mixing would also enhance the abnormally low calculated intensity in the simulated E component of the 3d <-- $1b_1$ cluster[18]. No doubt there is also p/d mixing in the excited state but it was less easy to find clear evidence of its likely magnitude. Hence only the above s/$d\sigma$ mixing was taken into account, with an energy independent strength which was taken to be common to the two series.

It should be noted in this context that Lee et.al.[21] find definitive evidence of s/p/d mixing in an ab initio based simulation of the ZEKE spectrum of H_2O[19]. In particular p-wave contributions to the photoorbital account very well for the occurrence of type-a lines in the observed spectrum that are forbidden by the nd <-- $1b_1$ propensity rule[2]. Secondly, certain ZEKE lines have mixed s/d contributions to their intensity while others appear as almost pure s <-- $1b_1$ lines. The latter might be seen as limiting lines in the ns <-- lb_1 series, whose n=3 and n=4 members are known[33,34], except that the implied quantum defect, $\mu(s) = 1.6$, would predict readily assignable ns($^1B_1$) <-- X($^1A_1$) bands well to the red of the complex (n-1)d <-- $1b_1$ bands in the present spectra. No such bands are observed; hence one must assume some mechanism for enhancing the ns <-- lb_1 intensity (relative to the nd <-- lb_1 bands) as n tends to infinity.

Limiting case (b) and case (d) assignments are shown in Figures 1(a), 2(a) and 2(g), but the assignment scheme used to optimize the quantum defects with an augmented *l* mixed version of the model of Child and Jungen[2] was based on the only three conserved quantities - the total angular momentum J and two parity labels, termed p and p^* by Gilbert et al.[18]. The quantum defects employed for the simulations, which are listed in Table 4, were separately optimized to the n=6 MPI and photoionization bands, whose close similarity suggests minimal effects from extraneous perturbations. Note however that the n=6 MPI assignment is ambiguous because two of the three strong lines around 98650 cm^{-1} and several weaker unassigned lines must be attributed to an overlapping system. Unfortunately the ambiguities cannot be resolved by use of combination differences because none are

predicted at the assumed beam temperature of 25 K. The assignment adopted was therefore based on the best fit, with standard deviation σ = 1.49 cm^{-1}, subject to reasonable consistency with the photoionization quantum defects and those obtained in earlier studies[2,18]. Given the assignments, values for the two ionization limits were obtained by including observed strong na and nb lines for $n \geq 9$ in the fit. The resulting values of 101773 cm^{-1} and 104985 cm^{-1} for the (000) and (100) limits agree well with the values of 101772 cm^{-1} and 104985 cm^{-1} obtained by Child and Jungen[2], but differ significantly from the current best literature values of 101766 cm^{-1} [19] and 104979 cm^{-1} obtained by adding ν_1 = 3213 cm^{-1} from Dinelli et. al.[35], presumably because the effects of l mixing have only partly been taken into account. Tables 1 and 2 list comparisons between the observed and calculated line positions, except that many of the photoionization lines for n=7 and 8 and a long series of weak lines for n=9, which are assumed to belong to overlapping series, have been omitted from the table.

The overall fit for the photoionization series is satisfactory given the presence of overlapping band for n=7 and n=8, which may also lead to bad perturbations. Differences between the quantum defects and those employed by Child and Jungen[2] arise from minor differences in the assignments suggested by the higher resolution of the present spectrum and from the present incorporation of s/dσ mixing. The situation with respect to the MPI series is less satisfactory. The assumption is that the strong na lines in the simulations for n=10-12 are removed by predissociation because their counterparts appear in the photoionization series and in the case (d) simulation. There is however only at best an accidental coincidence between the calculated and observed weak lines at these high n values. It is also extremely difficult to find a convincing simulation of the n=8 MPI band without assuming interaction with some presently unknown state.

Comparison with previous estimates for the quantum defects[2,18] is complicated by the facts that the effects of s/dσ mixing were not previously taken into account, and that the dπ^+ defect is relatively ill-determined by the present data. There are however significant changes in the (000) defects in passing from n=3[18] to the present high n values, particularly in the case of the dσ orbital, which would imply further changes as n increases. It is however unfortunately impossible to make sufficient confident assignments for high n members of the

MPI series to test this contention. Differences between the high n (000) and (100) defects are seen to lie outside the joint uncertainties only for the dσ and dδ orbitals. These could be reconciled by shifts of 8 cm^{-1} and 19 cm^{-1} in the relevent (000) electronic origins, of which the former could readily be accommodated by reassignment of the 6a line. Hence there is no definitive evidence from the n > 6 bands of any significant difference between the (000) and (100) quantum defects. Perceptible changes are however apparent between n=3 and n=6.

Some of the uncertainties raised by this preliminary analysis could be removed by further experiments.

i) More definitive assignments could be made either by raising the beam temperature or by repeating the present experiments with D_2O in order to allow the observation of ground state combination differences. Alternatively double resonance studies could be made via perhaps the well analysed[36] C $^1B_1$ state or by application of an ir-xuv ion depletion technique. Such improved assignments would be particularly valuable for the high n MPI series because they might provide firm evidence about d/p mixing in the excited state.

ii) It would be helpful to undertake a predissociation excitation search to yield H + OH(A) or O(^{1}D) + H_2 in the region of the nd(000) <-- $1b_1$ bands for n=10-12 in order to test the hypothesis that the strong na lines are lost by predissociation.

iii) Jet-cooled MPI experiments in the regions of the nd(000) <-- $1b_1$ and nd(100) <-- $1b_1$ bands for n=4 and 5 would be very helpful in assigning congested room temperature absorption spectra taken by Mayhew[37]. It would then be possible to follow changes in the quantum defects with n, in regions where the electronic band origins are most sensitive to such changes.

CONCLUDING REMARKS

In this paper new experimental results have been presented for one- and two-photon ionization of the water molecule involving resonant excitation to Rydberg levels converging on the (000) and (100) vibrational states of the H_2O^+ ion, respectively. The experimental results have been analyzed by applying multichannel quantum defect theory (MQDT). The MQDT analysis suggests that Rydberg molecules in states with intermediately high principal quantum numbers, like the ones studied here, are near Hund's case (d), where the excited nd orbitals are near degenerate on the scale of the rotational constants. The nd components are still well separated from the ns and np components. Therefore, Coriolis coupling between the different ns, np and nd components is negligible. Within the nd manifold however, for n=9-12, the reduction in the Coriolis coupling towards higher n points towards some ndσ/ns mixing. A pure case (d) spectrum is anticipated at even higher principal quantum numbers, when the separations between all electronic origins become negligible.

A comparison of the experimental results and the MQDT simulations shows that some serious discrepancies have remained. A few possible explanations have been offered. First of all, a comparison of the experimental results for n=6 in the one- and two-photon ionization, suggests that the two-photon ionization results, in which the molecule is initially excited below the first ionization threshold, may be subject to the influences of selective predissociation. And secondly, it is believed that a significant role in explaining the remaining discrepancies is played by the interaction between bent and linear Rydberg states. The ab-initio bending potential curves calculated by Hirst and Child[23)] show a large number of avoided crossings between diabatic curves related to bent states describing excitations of the $1b_1$ non-bonding orbital and diabatic curves related to linear states describing excitations of the $3a_1$ bonding orbital. In particular, Hirst and Child pointed out that the diabatic bending potential energy curve for $3pb_2$ <-- $3a_1$ ($^1B_2$) excitation cuts through all the nda_2 <-- $1b_1$ ($^1B_2$) diabatic bending potential energy curves close to their equilibrium bending angle. Since, as pointed out above, all the nd components of different symmetry are coupled through the Coriolis forces on the Rydberg electron, the $3pb_2$ <-- $3a_1$ ($^1B_2$) state would be a prime candidate to perturb the entire spectrum. Experimental credibility for this argument

is given by the fact that both the positions and the lifetimes of some of the observed Rydberg progressions show irregular behaviour for certain values of the principal quantum number. Incorporation of the bent-linear interactions in a quantum defect treatment remains to be done.

ACKNOWLEDGEMENTS

M.V. wishes to acknowledge Dr. Evan F. Cromwell and Dr. Andrew H. Kung for the development of the ultra-high resolution xuv laser system used in these experiments, and Dr. Laurent Nahon for reading the manuscript prior to publication.

This work was supported by the Director, Office of Energy Research, Office of Basic Energy Sciences, Chemical Sciences Division, of the U.S. Department of Energy under Contract No. DE-AC03-76SF00098.

REFERENCES

1) R.H. Page and R.J. Larkin, Y.R. Shen and Y.T. Lee, J. Chem. Phys. 88, 2249 (1988).
2) M.S. Child and Ch. Jungen, J. Chem. Phys. 93, 7756 (1990).
3) M.J. Seaton, Rep. Prog. Phys. 46, 167 (1983).
4) U. Fano, Phys. Rev. 2, 353 (1970).
5) Ch.H. Greene and Ch. Jungen, Adv. At. Mol. Phys. 21, 51 (1985).
6) W.C. Price, J. Chem. Phys. 4, 147 (1936).
7) W.A. Goddard III and W.J. Hunt, Chem. Phys. Lett. 24, 464 (1974).
8) M.B. Robin, "Higher Excited States of Polyatomic Molecules", (Academic, New York, 1974).
9) D.H. Katayama, R.E. Huffman and C.L. O'Bryan, J. Chem. Phys. 59, 4309 (1973).
10) G.H.F. Diercksen, W.P. Kraemer, T.N. Rescigno, C.F. Bender, B.V. McKoy, S.R. Langhoff and P.W. Langhoff, J. Chem. Phys. 76, 1043 (1982).
11) E. Ishiguro, M. Sasanuma, H. Masuko, Y. Morioka and M. Nakamura, J. Phys. B: Atom. Molec. Phys. 11, 993 (1978).
12) P. Gürtler, V. Saile and E.E. Koch, Chem. Phys. Lett. 51, 386 (1977).
13) P.R. Bunker, "Molecular Symmetry and Spectroscopy", (Academic, New York, 1979).
14) J.P. Connerade, M.A. Baig, S.P. McGlynn and W.R.S. Garton, J. Phys. B, 13, L705 (1980).
15) C.A. Mayhew, PhD. thesis, Imperial College of Science, London (1984).
16) P.L. Smith, K. Yoshino, H.E. Griesinger and J.H. Black, Astrophy. J. 250, 166 (1981).
17) M.N.R. Ashfold and J.M. Bayley, J. Chem. Soc. Faraday. Trans. 86, 213 (1990).
18) R.D. Gilbert, M.S. Child and J.W.C. Johns, Mol. Phys. 74, 473 (1991).
19) R.G. Tonkyn, R. Wiedmann, E.R. Grant and M.G. White, J. Chem. Phys. 95, 7033 (1991).
20) R.D. Gilbert and M.S. Child, Chem. Phys. Lett. 287, 153 (1991).
21) M.-T. Lee, K. Wang, V. McKoy, R.G. Tonkyn, R.T. Wiedmann, E.R. Grant and M.G. White, J. Chem. Phys. 96, 7848 (1992).
22) H.-T. Wang, W.S. Felps and S.P. McGlynn, J. Chem. Phys. 67, 2614 (1977).
23) D.M. Hirst and M.S. Child, Mol. Phys. (in press).

24) M.N.R. Ashfold, J.M. Bayley and R.N. Dixon, Chem. Phys. 84, 35 (1984).

25) O. Dutuit, A. Tabche-Fouhaile, I. Nenner, H. Frohlich and P.M. Guyon, J. Chem. Phys. 83, 584 (1985).

26) T.G. Schlanger and G. Black, J. Chem. Phys. 77, 2432 (1982).

27) Ch. Jungen, K.E.J. Hallin and A.J. Merer, Mol. Phys, 40, 65 (1980).

28) a) E. Cromwell, T. Trickl, Y.T. Lee and A.H. Kung, Rev. Sci. Instrum. 60, 2888 (1989).

b) E. Cromwell, PhD thesis, University of California at Berkeley (1991).

29) R.H. Page, R.J. Larkin, A.H. Kung, Y.R. Shen and Y.T. Lee, Rev. Sci. Instum. 58, 1616 (1987).

30) D. Proch and T. Trickl, Rev. Sci. Instrum. 60, 713 (1989).

31) T. Trickl, M.J.J. Vrakking, E. Cromwell, Y.T. Lee and A.H. Kung, Phys. Rev. A 39, 2948 (1989).

32) J.K.G. Watson, J. Chem. Phys. 46, 1946 (1967).

33) G. Herzberg, "Electronic spectra of polyatomic molecules", (Van Nostrand, 1967).

34) M.N.R. Ashfold, J.M. Bayley and R.N. Dixon, Can. J. Phys. 62, 1806 (1984).

35) B.M. Dinelli, M.W. Crofton and T. Oka, J. Mol. Spectr. 127, 1 (1988).

36) J.W.C. Johns, Can. J. Phys. 49, 944 (1971).

37) C. Mayhew (private communication).

Table 1: Observed and calculated MPI line positions.
Experimental lines marked * were used in the quantum defect optimization.

Experimental line position (cm^{-1})	Calculated line position (cm^{-1})	Calculated intensity (a.u.)	Assignment $\{J,p,p^*\}$ <-- $J(K_aK_c)$
	n=6		
98589.94	98579.43	0.18	{0,0,0} <-- 1(10)
98606.80	98606.36	0.04	{1,1,1} <-- 1(11)
98628.16 *	98627.80	0.38	{2,0,0} <-- 1(10)
	98638.21	0.75	{1,0,1} <-- 1(01)
98647.26 *	98648.42	2.17	{2,0,1} <-- 1(01)
98647.26	98649.71	0.39	{1,1,0} <-- 0(00)
98654.43			
98658.57			
98674.00			
98682.20			
98697.01	98695.32	0.12	{2,1,1} <-- 1(11)
98699.46	98699.45	0.78	{2,0,0} <-- 1(10)
98710.82 *	98712.11	0.09	{2,0,0} <-- 1(10)
98719.12 *	98718.99	0.57	{0,0,1} <-- 1(01)
98722.58			
98731.18			
98734.39			
98745.29	98743.23	0.40	{1,0,0} <-- 1(10)
98745.29 *	98746.97	0.50	{1,1,0} <-- 0(00)
98748.55	98749.28	1.72	{1,0,1} <-- 1(01)
98758.65 *	98755.06	1.18	{2,0,1} <-- 1(01)
98787.37			

98810.59 *	98810.45	0.20	{0,0,0} <-- 1(10)
98825.60	98826.66	0.15	{1,0,0} <-- 1(10)
98828.15			
98832.95			
	98839.84	0.23	{2,0,1} <-- 1(10)
98865.41			
98873.81			
98879.62			
	n=7		
99432.58	99426.57	0.34	{2,0,1} <-- 1(01)
99489.52			
99500.03	99500.79	0.27	{2,0,0} <-- 1(10)
99503.93	99508.09	0.48	{1,0,1} <-- 1(01)
99503.93	99510.84	1.54	{2,0,1} <-- 1(01)
99512.44	99511.38	0.31	{1,1,0} <-- 0(00)
99526.35	99523.93	0.40	{2,0,0} <-- 1(10)
99549.26	99553.43	0.36	{0,0,1} <-- 1(01)
99559.47	99563.98	1.09	{1,0,1} <-- 1(01)
99566.53			
99569.53	99570.74	0.24	{1,1,0} <-- 0(00)
99573.28	99577.14	0.28	{1,0,0} <-- 1(10)
99578.69	99583.99	0.46	{2,0,1} <-- 1(01)
99620.92	99622.40	0.13	{0,0,0} <-- 1(10)
99626.92			
99634.52			
99637.13			
99641.53	99642.16	0.07	{1,0,0} <-- 1(10)

	n=8		
100017.42	100014.71	0.65	{2,0,1} <-- 1(01)
100021.62			
100056.14	100054.81	0.13	{2,0,0} <-- 1(10)
100058.60			
100059.95	100063.25	0.25	{1,1,0} <-- 0(00)
100069.96	100067.28	0.28	{2,0,0} <-- 1(10)
100069.96	100068.04	0.37	{1,0,1} <-- 1(01)
100069.96	100068.31	0.89	{2,0,1} <-- 1(01)
100076.91			
100082.21			
	100092.72	0.24	{0,0,1} <-- 1(01)
100097.98	100093.17	0.69	{1,0,1} <-- 1(01)
100116.44	100117.19	0.21	{1,0,0} <-- 1(10)
	100123.49	0.15	{2,0,1} <-- 1(01)
100131.00			
100136.50			
100196.79			
	n=9		
100342.89	100337.41	0.09	{2,0,0} <-- 1(10)
100407.53	100407.70	0.84	{2,0,1} <-- 1(01)
100436.05	100437.46	0.20	{1,1,0} <-- 0(00)
100451.17 *	100448.64	0.52	{2,0,1} <-- 1(01)
100451.17	100451.49	0.37	{1,0,1} <-- 1(01)
	100453.93	0.17	{0,0,1} <-- 1(01)
	100454.32	0.19	{2,0,0} <-- 1(10)
	100457.81	0.25	{1,0,1} <-- 1(01)

	100461.26	0.17	{0,0,1} <-- 1(01)
	100486.79	0.17	{1,0,0} <-- 1(10)
	n=10		
100648.25			
100663.41			
	100676.45	0.71	{2,0,1} <-- 1(01)
100693.03			
	100702.73	0.16	{1,1,0} <-- 0(00)
100711.79 *	100712.27	0.25	{2,0,1} <-- 1(01)
100711.79	100713.91	0.58	{1,0,1} <-- 1(01)
100716.85			
	100724.21	0.12	{0,0,1} <-- 1(01)
	100729.69	0.17	{2,0,0} <-- 1(10)
100742.76			
	100750.72	0.14	{1,0,0} <-- 1(10)
	n=11		
100808.35	100811.56	0.07	{2,0,0} <-- 1(10)
100808.35	100811.56	0.17	{2,0,1} <-- 1(01)
100827.11			
100843.72			
100848.43			
	100858.34	0.24	{2,0,1} <-- 1(01)
100867.64	100871.84	0.23	{2,0,1} <-- 1(01)
100897.41	100897.76	0.13	{1,1,0} <-- 0(00)
	100900.10	0.27	{2,0,1} <-- 1(01)
100907.36 *	100907.31	0.46	{1,0,1} <-- 1(01)

100909.31			
	100918.36	0.09	{0,0,1} <-- 1(01)
	100932.15	0.14	{2,0,0} <-- 1(10)
	100945.60	0.11	{1,0,0} <-- 1(10)
n=12			
100983.07	100983.02	0.11	{2,0,1} <-- 1(01)
100996.88			
101009.49			
101023.00	101020.80	0.39	{2,0,1} <-- 1(01)
101037.26			
101042.91	101045.42	0.10	{1,1,0} <-- 0(00)
101053.72 *	101053.15	0.40	{1,0,1} <-- 1(01)
	101058.88	0.10	{2,0,1} <-- 1(01)
	101062.01	0.05	{2,0,0} <-- 1(10)
	101065.78	0.07	{0,0,1} <-- 1(01)
101072.88	101076.66	0.07	{2,0,0} <-- 1(10)
101098.76			

Table 2: Observed and calculated photoionizaton line positions.
Lines marked * were used to optimize the quantum defects.
Lines thought to belong to other band systems have been omitted.

Experimental line position (cm^{-1})	Calculated line position (cm^{-1})	Calculated intensity (a.u.)	Assignment $\{J,p,p^*\}$ <-- $J(K_aK_c)$
	n=6		
101799.62 *	101797.65	0.17	{0,0,0} <-- 1(10)
101811.07			
101818.15			
101848.30 *	101847.06	0.38	{2,0,0} <-- 1(10)
101855.26 *	101856.14	0.76	{1,0,1} <-- 1(01)
101862.14 *	101864.35	2.20	{2,0,1} <-- 1(01)
101864.62	101865.55	0.41	{1,1,0} <-- 0(00)
101870.46			
101914.71 *	101914.73	0.70	{2,0,0} <-- 1(10)
101922.13 *	101923.46	0.57	{0,0,1} <-- 1(01)
101929.44 *	101930.57	0.16	{2,0,0} <-- 1(10)
101941.42			
101947.38 *	101950.17	0.37	{1,0,0} <-- 1(10)
101959.28 *	101959.68	0.45	{1,1,0} <-- 0(00)
101968.20 *	101967.74	1.71	{1,0,1} <-- 1(01)
101970.27 *	101969.31	1.03	{2,0,1} <-- 1(01)
102018.90 *	102019.11	0.20	{0,0,0} <-- 1(10)
102100.71			
102039.69			
	102048.74	0.32	{2,0,1} <-- 1(01)
	102049.95	0.17	{1,0,0} <-- 1(10)

	n=7		
	102651.64	0.42	{2,0,1} <-- 1(01)
	102662.23	0.11	{0,0,0} <-- 1(10)
	102718.12	0.22	{2,0,0} <-- 1(10)
102721.05	102722.67	0.49	{1,0,1} <-- 1(01)
	102723.74	0.31	{1,1,0} <-- 0(00)
102726.68	102724.84	1.47	{2,0,1} <-- 1(01)
102735.79	102739.45	0.45	{2,0,0} <-- 1(10)
102758.64	102759.23	0.36	{0,0,1} <-- 1(01)
102777.70	102779.09	1.07	{1,0,1} <-- 1(01)
	102784.11	0.23	{1,1,0} <-- 0(00)
102789.50	102785.69	0.27	{1,0,0} <-- 1(10)
102798.81	102797.77	0.42	{2,0,1} <-- 1(01)
102830.29	102830.42	0.13	{0,0,0} <-- 1(10)
102859.81			
	n=8		
103216.49	103218.16	0.07	{0,0,0} <-- 1(10)
103254.18			
103259.36			
	103228.49	0.67	{2,0,1} <-- 1(01)
	103267.55	0.10	{2,0,0} <-- 1(10)
	103274.01	0.25	{1,1,0} <-- 0(00)
103278.61	103280.66	0.81	{2,0,1} <-- 1(01)
	103280.73	0.41	{1,0,1} <-- 1(01)
	103283.62	0.31	{2,0,0} <-- 1(10)
103298.23	103299.26	0.24	{0,0,1} <-- 1(01)
103306.10	103306.65	0.65	{1,0,1} <-- 1(01)

103309.42			
103323.45	103326.76	0.20	{1,0,0} <-- 1(10)
	103335.37	0.15	{2,0,1} <-- 1(01)
103341.38			
	n=9		
103616.54 *	103616.54	0.78	{2,0,1} <-- 1(01)
	103647.53	0.20	{1,1,0} <-- 0(00)
103661.51 *	103659.65	0.56	{1,0,1} <-- 1(01)
103661.51	103660.75	0.36	{2,0,1} <-- 1(01)
	103668.16	0.20	{2,0,0} <-- 1(10)
	103668.25	0.17	{0,0,1} <-- 1(01)
103670.15	103670.91	0.21	{1,0,1} <-- 1(01)
103688.18			
103695.07	103696.84	0.16	{1,0,0} <-- 1(10)
103701.42			
103707.90			
	n=10		
103838.84			
103860.17			
103869.51			
103878.56			
103886.66 *	103884.27	0.66	{2,0,1} <-- 1(01)
103904.93			
103907.99			
103911.82	103912.73	0.15	{1,1,0} <-- 0(00)
103917.90			

	103922.60	0.25	{2,0,1} <-- 1(01)
103925.26 *	103924.26	0.58	{1,0,1} <-- 1(01)
103926.77			
103931.59	103931.48	0.12	{0,0,1} <-- 1(01)
	103941.39	0.16	{2,0,0} <-- 1(10)
	103960.84	0.13	{1,0,0} <-- 1(10)
	n=11		
103980.68	103983.05	0.13	{1,0,1} <-- 1(01)
103986.68			
103991.64			
103992.77			
	104019.64	0.18	{2,0,1} <-- 1(01)
	104068.60	0.19	{2,0,1} <-- 1(01)
104079.11 *	104079.39	0.26	{2,0,1} <-- 1(01)
104102.21			
	104107.38	0.13	{1,1,0} <-- 0(00)
104107.99	104109.54	0.27	{2,0,1} <-- 1(01)
104113.88 *	104117.42	0.47	{1,0,1} <-- 1(01)
104128.06			

Table 3: Linewidths for na/nb series converging on $H_2O^+(000)$ and $H_2O^+(100)$ (in cm^{-1})		
Peak	$H_2O^+(000)$ [MPI]	$H_2O^+(100)$ [Direct photoionization]
6a	1.3	2.8
6b	1.3	1.3
7a	1.0	3.0
7b	1.8	2.1
8a	3.5	
8b	0.5	~ 4.5
9a	[1.5]	2.3
9b	1.1	2.2
10a	0.7	1.5
10b		2.0
11a	0.9	1.4
11b		1.4
12b	0.6	
13b	0.6	

Table 4: Parameters for the quantum defect simulation				
State orbital	$\mu(000)$ n=3 [a)]	$\mu(000)$ n=6-12	$\mu(100)$ n=6-11	$\mu(100)$ [b)]
D'^1B_1 s		[1.6274]	[1.6274]	
E^1B_1 $d\sigma$	0.1243	0.1511(63)	0.1423(11)	0.155(5)
E'^1B_2 $d\pi^-$	0.0771	0.0670(18)	0.0704(13)	0.067(7)
D''^1A_2 $d\pi^+$	0.3463	0.3607(548)	0.3196(140)	0.327(32)
F^1B_1 $d\delta^+$	-0.0124	0.0086(20)	0.0068(20)	0.007(10)
$^1A_1$ $d\delta^-$	-0.0145	0.0179(47)	-0.0008(35)	0.013(9)
s/$d\sigma$ mixing angle [c)]	0.0	0.1π	0.1π	0.0
IP/cm^{-1}	101773.0	101773.0	104983.0	104985.0
Ry/cm^{-1}	109733.8	109733.8	109733.8	109733.8

a) Gilbert, Child and Johns[18)]

b) Child and Jungen[2)]

c) $|d\sigma'\rangle = \cos\vartheta\ |d\sigma\rangle + \sin\vartheta\ |s\rangle$

FIGURE CAPTIONS

Figure 1 Observed (upper panel) and simulated (lower panel) MPI spectra for n=6-12. The simulation employs a Lorentzian profile with FWHM = 1.0 cm^{-1}. Assignments given for n=6 represent the dominate case (b) component of the wavefunction. Those marked ? are too heavily mixed by Coriolis coupling to be assignable. The designation $d_2 1_{1-}$ etc. implies complete Coriolis coupling between the F components[23].

Figure 2 Observed (upper panel) and simulated (lower panel) photoionization spectra for n=6-11, 2a to 2f respectively, plus a case (d) simulation in figure 2g obtained by switching off the s/dσ mixing and by setting all quantum defects to zero. The simulation employs a Lorentzian profile with FWHM 2.0 cm^{-1}. Assignments given for n=6 represent the dominate case (b) component of the wavefunction. The designation $d_2 1_{1-}$ etc. implies complete Coriolis coupling between the two F components[23].

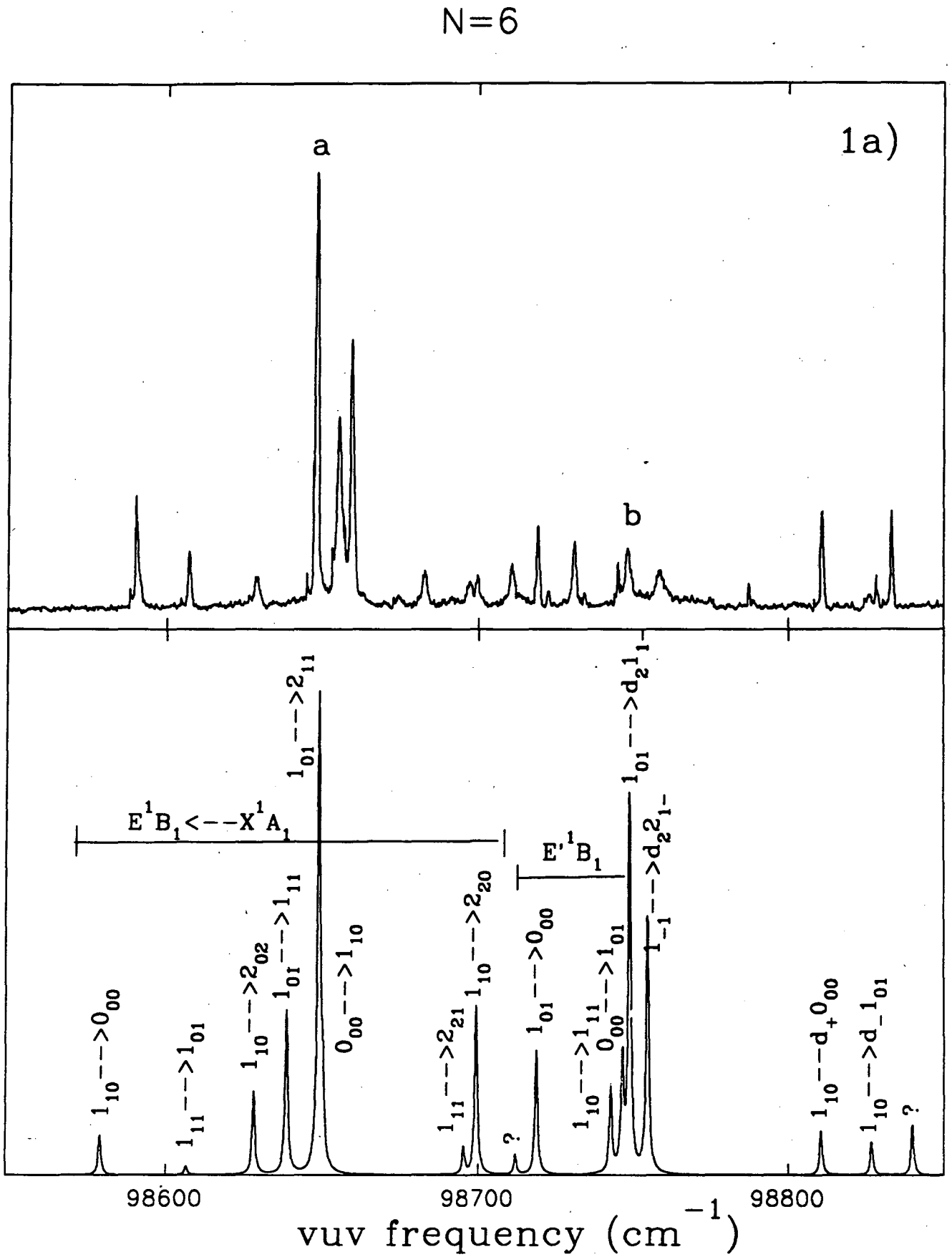
N=6
1a)
a
b
$E^1B_1 <--- X^1A_1$
E'^1B_1
$1_{10} -->0_{00}$
$1_{11} -->1_{01}$
$1_{10} -->2_{02}$
$1_{01} -->1_{11}$
$1_{01} -->2_{11}$
$0_{00} -->1_{10}$
$1_{11} -->2_{21}$
$1_{10} -->2_{20}$
?
$1_{01} -->0_{00}$
$1_{10} -->1_{11}$
$0_{00} -->1_{01}$
$1_{01} -->d_2 1_1$
$1_{-1} -->d_2 2_{1-}$
$1_{10} -- d_+ 0_{00}$
$1_{10} -->d_- 1_{01}$
?
98600
98700
98800
vuv frequency (cm^{-1})

Fig. 1(a)

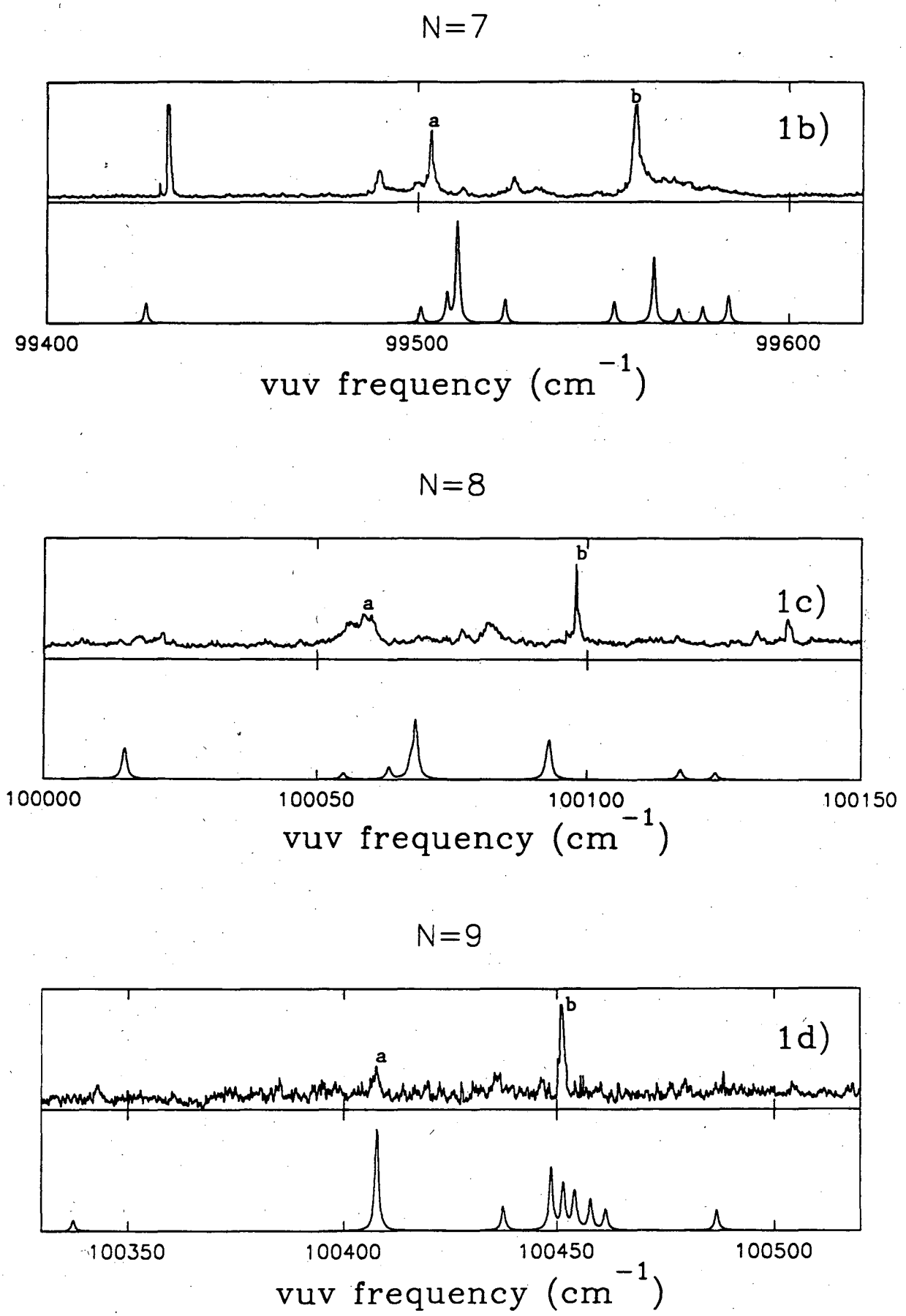
N=7
a
b
1b)
99400
99500
99600
vuv frequency (cm^{-1})
N=8
a
b
1c)
100000
100050
100100
100150
vuv frequency (cm^{-1})
N=9
a
b
1d)
100350
100400
100450
100500
vuv frequency (cm^{-1})

Fig. 1(b-d)

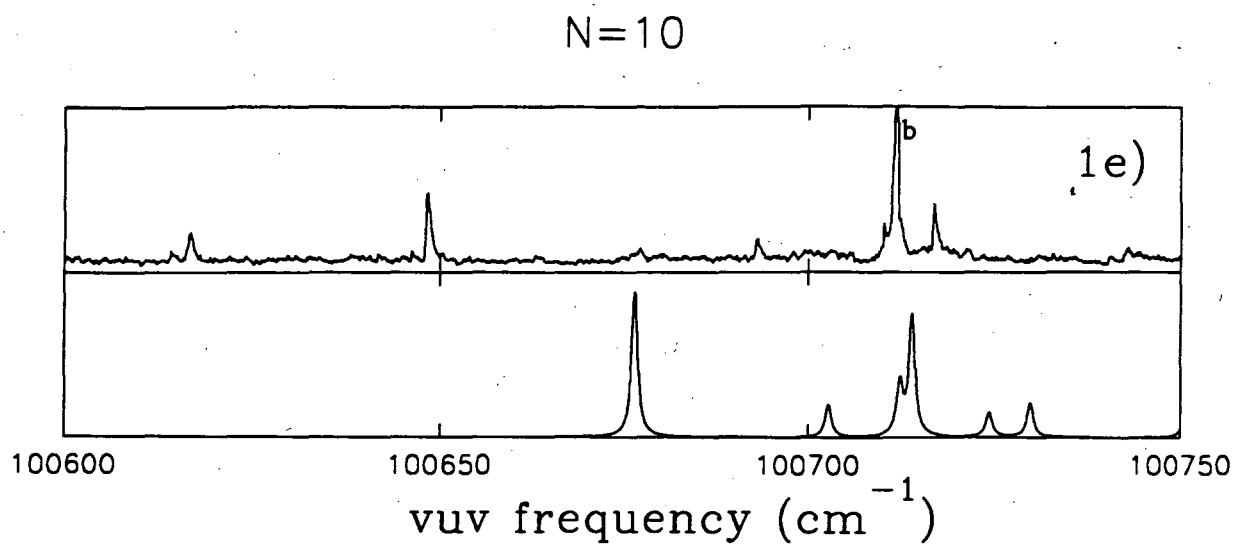
N=10
b
1e)
100600
100650
100700
100750
vuv frequency (cm^{-1})

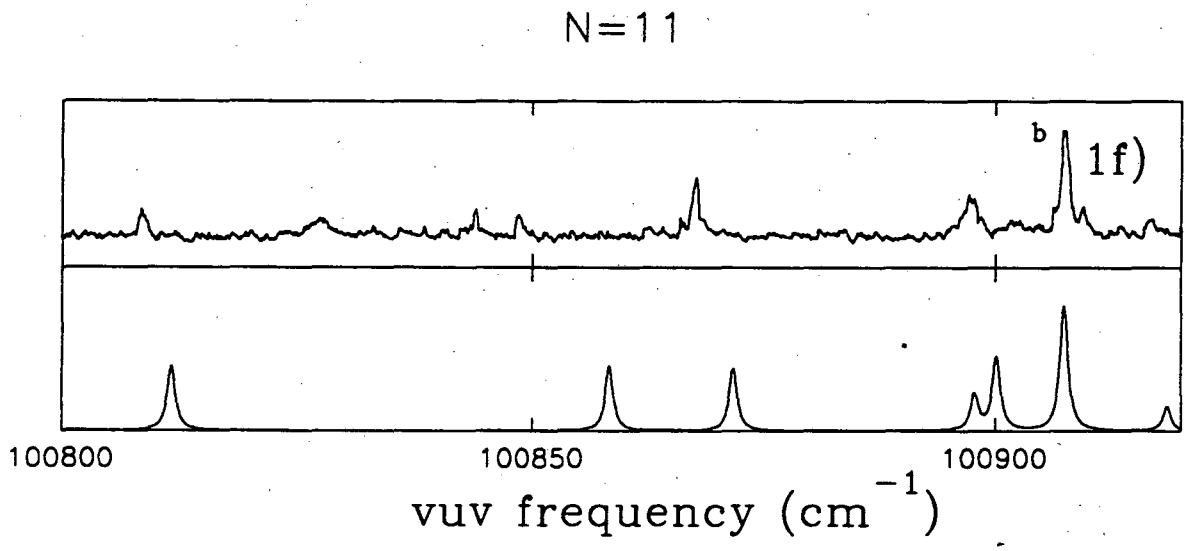
N=11
b
1f)
100800
100850
100900
vuv frequency (cm^{-1})

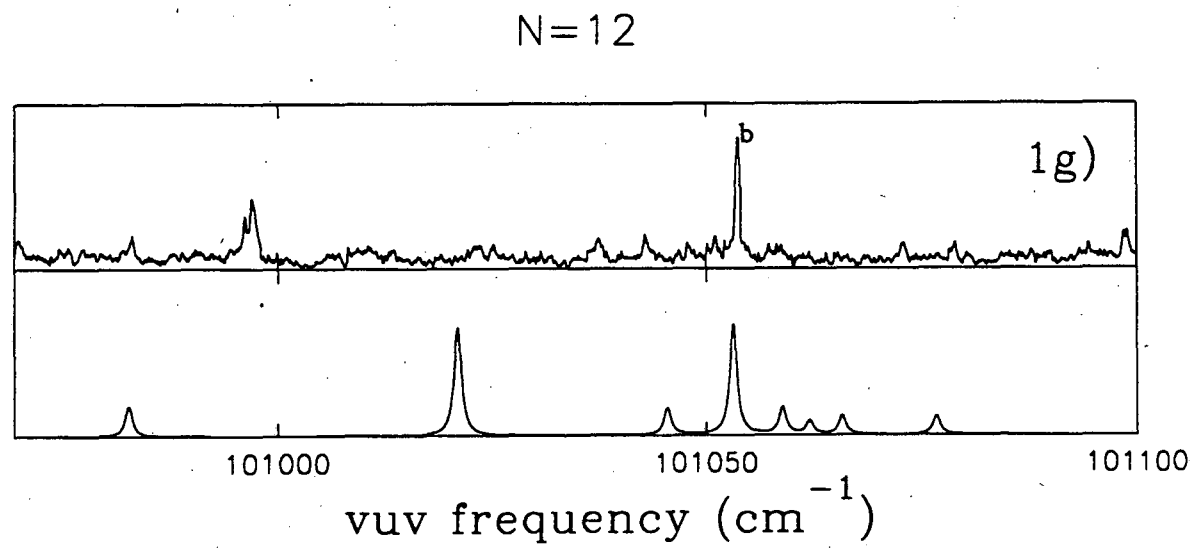
N=12
b
1g)
101000
101050
101100
vuv frequency (cm^{-1})

Fig. 1(e-g)

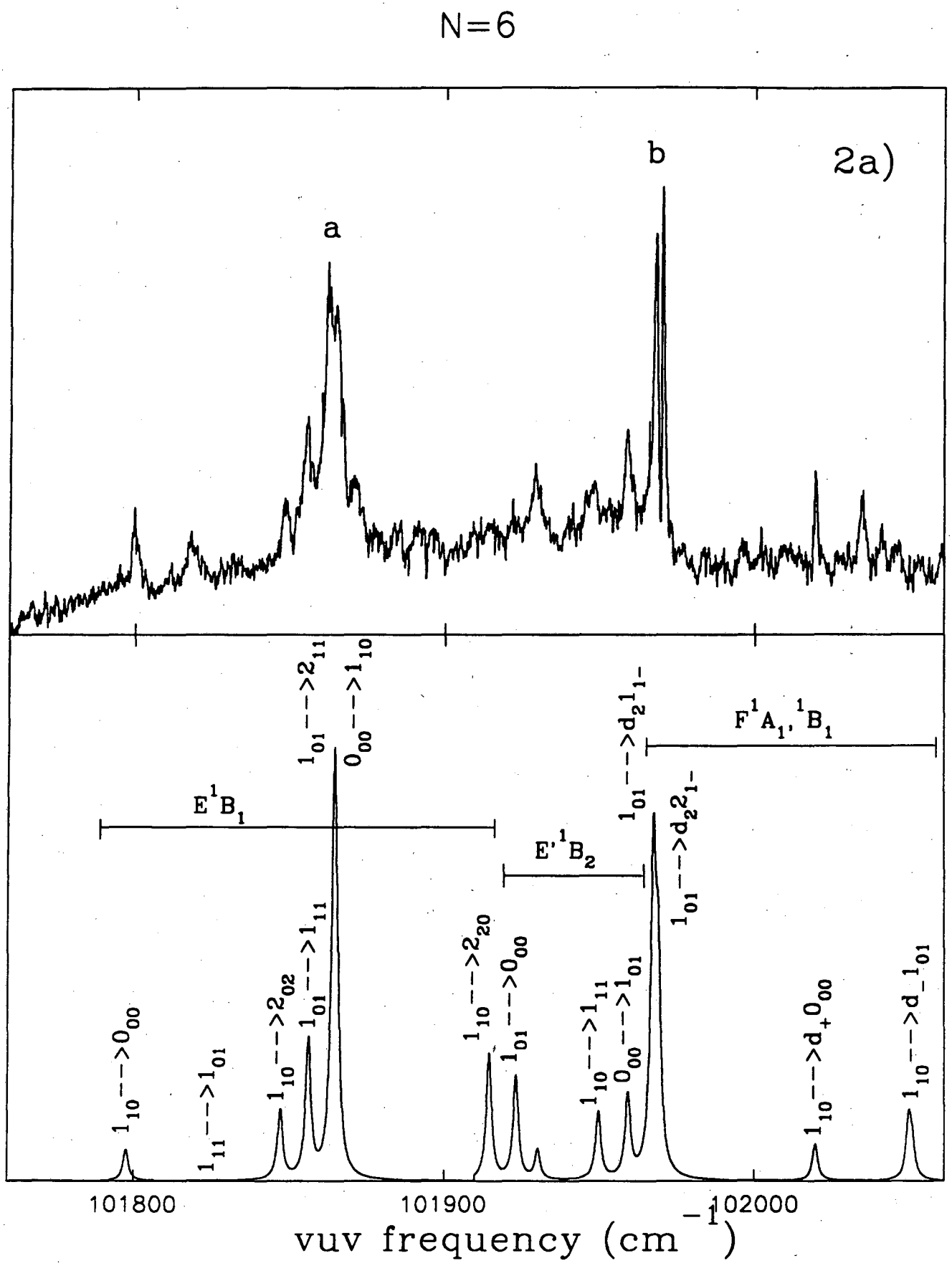
N=6
2a)
a
b
E^1B_1
E'^1B_2
$F^1A_1, {}^1B_1$
1_{10}-->0_{00}
1_{11}-->1_{01}
1_{10}-->2_{02}
1_{01}-->1_{11}
1_{01}-->2_{11}
0_{00}-->1_{10}
1_{10}-->2_{20}
1_{01}-->0_{00}
1_{10}-->1_{11}
0_{00}-->1_{01}
1_{01}-->$d_2 2_{1-}$
1_{01}-->$d_2 1_{1-}$
1_{10}-->$d_+ 0_{00}$
1_{10}-->$d_- 1_{01}$
101800
101900
102000
vuv frequency (cm^{-1})

Fig. 2(a)

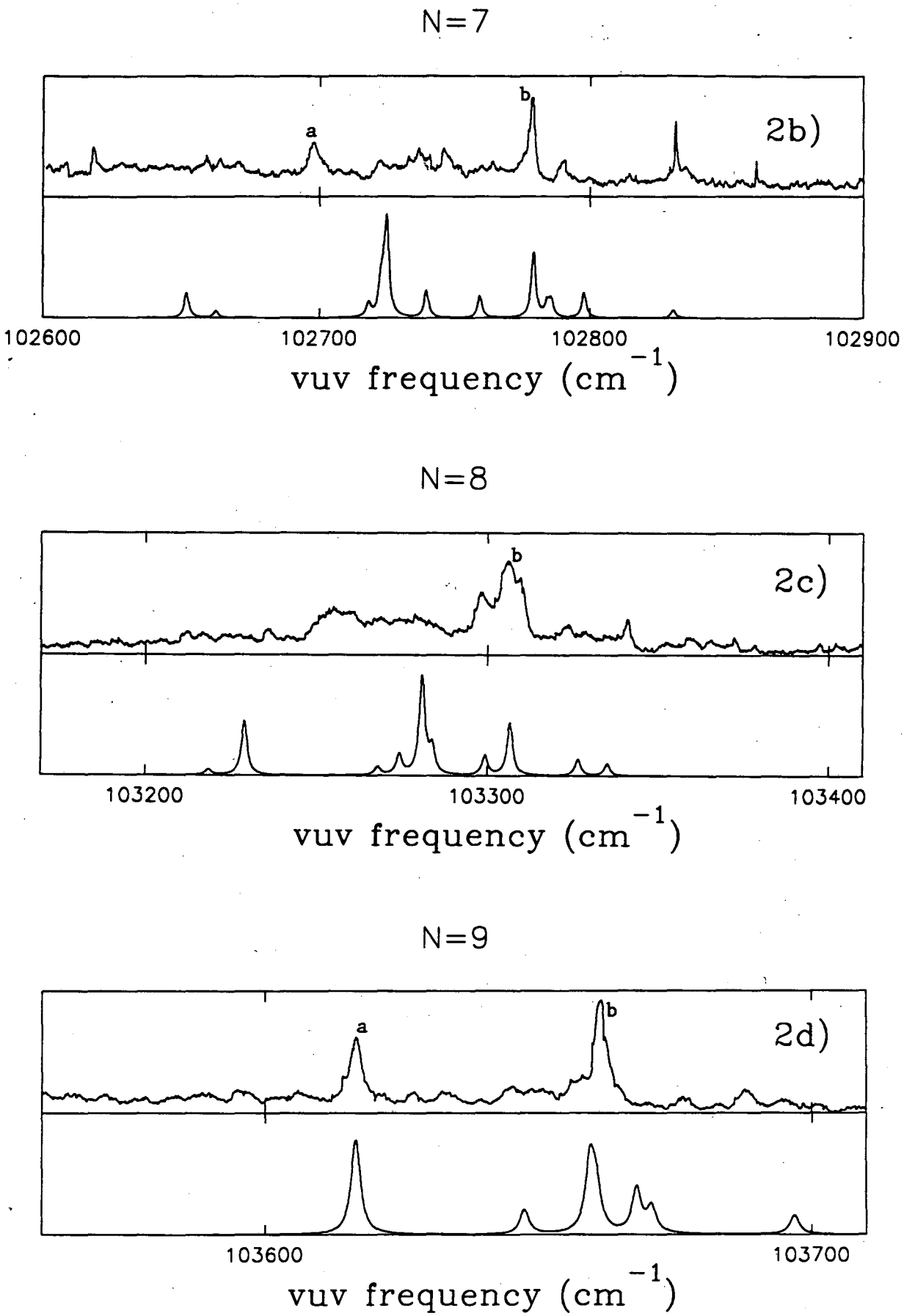
N=7
a
b
2b)
102600
102700
102800
102900
vuv frequency (cm^{-1})
N=8
b
2c)
103200
103300
103400
vuv frequency (cm^{-1})
N=9
a
b
2d)
103600
103700
vuv frequency (cm^{-1})

Fig. 2(b-d)

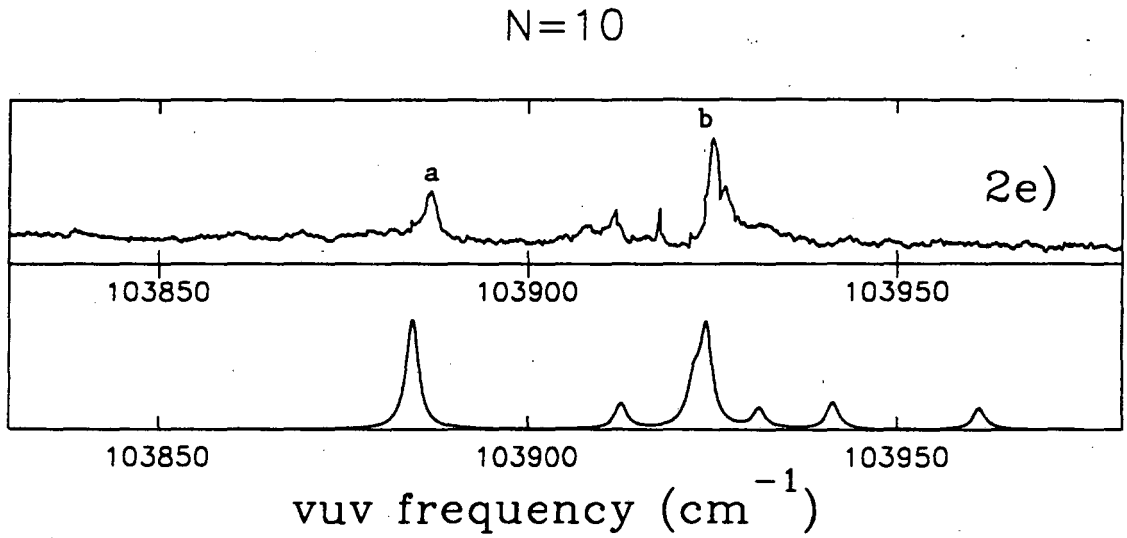
N=10
a
b
2e)
103850
103900
103950
103850
103900
103950
vuv frequency (cm^{-1})

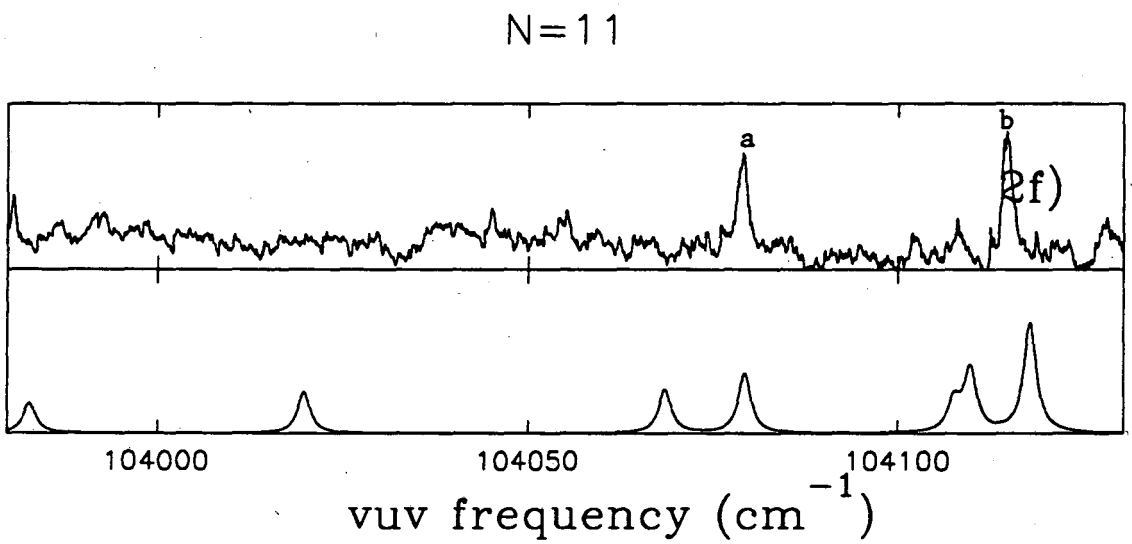
N=11
a
b
2f)
104000
104050
104100
vuv frequency (cm^{-1})

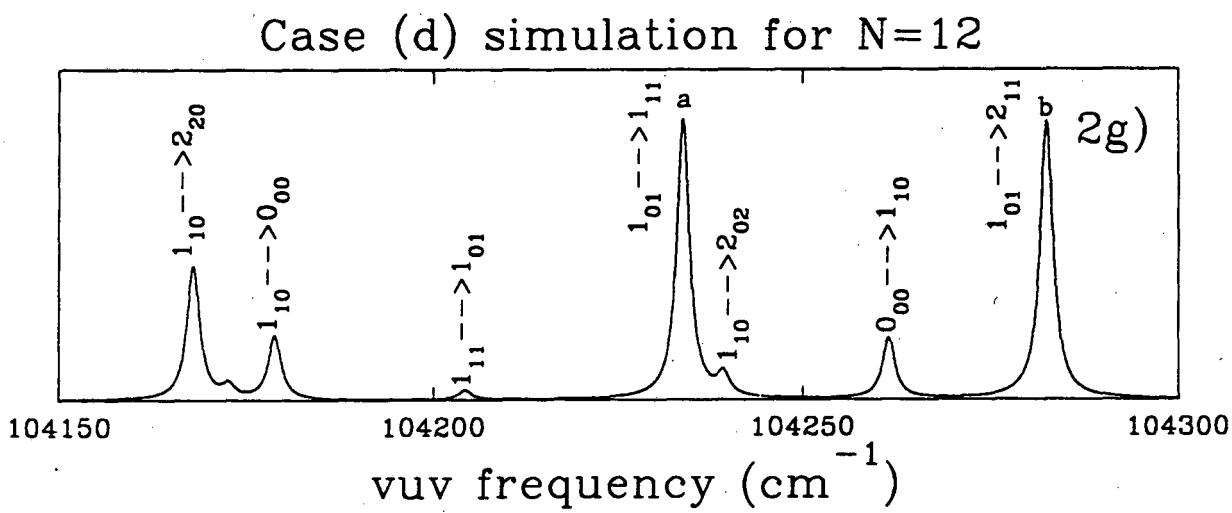
Case (d) simulation for N=12
1_{10}-->2_{20}
1_{10}-->0_{00}
1_{11}-->1_{01}
1_{01}-->1_{11}
a
1_{10}-->2_{02}
0_{00}-->1_{10}
1_{01}-->2_{11}
b
2g)
104150
104200
104250
104300
vuv frequency (cm^{-1})

Fig. 2(e-g)

LAWRENCE BERKELEY LABORATORY
UNIVERSITY OF CALIFORNIA
TECHNICAL INFORMATION DEPARTMENT
BERKELEY, CALIFORNIA 94720